

# Identifying Topological Order by Measuring the Modular Matrices

Zhihuang Luo<sup>1,2</sup>, Jun Li<sup>2</sup>, Zhaokai Li<sup>1</sup>, Ling-Yan Hung<sup>3,4,5\*</sup>, Yidun Wan<sup>3,4,5,6\*</sup>, Xinhua Peng<sup>1,7\*</sup>,  
& Jiangfeng Du<sup>1,7</sup>

<sup>1</sup>*Hefei National Laboratory for Physical Sciences at Microscale and Department of Modern Physics, University of Science and Technology of China, Hefei, Anhui 230026, China*

<sup>2</sup>*Beijing Computational Science Research Center, Beijing, 100094, China*

<sup>3</sup>*State Key Laboratory of Surface Physics and Department of Physics, Fudan University, 220 Handan Road, 200433 Shanghai, China*

<sup>4</sup>*Department of Physics and Center for Field Theory and Particle Physics, Fudan University, 220 Handan Road, 200433 Shanghai, China*

<sup>5</sup>*Collaborative Innovation Center of Advanced Microstructures, Nanjing University, Nanjing, 210093, China*

<sup>6</sup>*Perimeter Institute for Theoretical Physics, Waterloo, Ontario N2L 2Y5, Canada*

<sup>7</sup>*Synergetic Innovation Center of Quantum Information and Quantum Physics, University of Science and Technology of China, Hefei, Anhui 230026, China*

**The modern conception of phases of matter has undergone tremendous developments since the first observation of topologically ordered state in fractional quantum Hall systems in the 1980s. Topological orders are exotic states of matter characterized by patterns of long-range entanglement that lie beyond Landau's symmetry breaking paradigm. In 2+1 dimen-**

sions, these phases support signature anyonic excitations with fractional statistics or even non-Abelian braiding effects. One important theoretical question is how we should characterize these phases. In 2+1 dimensions, plenty of evidence suggests that the *modular matrices*,  $S$  and  $T$ , suffice to characterize the order completely. It is thus of equal importance to find out if these quantities are experimental observables. Here we demonstrate how such measurements can indeed be achieved using only the given Hamiltonian, allowing one to identify the corresponding topological order using a nuclear magnetic resonance simulator. This is a first experimental realization of these fundamental signatures of a topological order; it opens up new future avenues toward identifying more generic topological orders based purely on experimental measurements.

Landau's theory fails to describe many exotic phases of matter such as topological orders, where no symmetry breaking is involved<sup>1-4</sup>. Topological orders are characterized by their robust ground-state degeneracy and long-range entanglement<sup>5,6</sup>. The fractional quantum Hall states are among the best known examples of such states<sup>7</sup>. It is well known that topological orders do not admit any local order parameters. Characterization based on quantities such as topological entanglement entropy<sup>21,23</sup> has also proved inadequate, as they often take the same value for different phases. It is thus a profound and important quest to identify the minimal set of topological observables that would uniquely identify these phases.

Recent theoretical works show that modular matrices might help achieve precisely this goal<sup>9-16</sup>. More specifically, imagine placing a two-dimensional system on a torus, which practically

corresponds to periodic boundary conditions along two independent cycles. The S and T modular matrices are Berry phases accumulated when one adiabatically deforms the system geometrically. S corresponds to a  $\pi/2$  rotation, and T to a shear – often called a Dehn twist – of the fundamental region of the torus, as illustrated in Fig. 1. Generically, there are multiple ground states on a torus, and the modular matrices furnish non-Abelian representation of the modular group  $SL(2, \mathbb{Z})$ , and are thus instances of non-Abelian geometric phases. Like a fingerprint, they can be used to uniquely distinguish different topological orders. For example,  $Z_2$  states and the Fibonacci state have different modular matrices. And from these modular matrices, their anyonic statistic can be obtained, which can be seen in Supplementary Information, as well as some further details on theoretical description of the modular matrices.

Numerically, modular matrices can be computed from ground-state wave-function overlap, which is employed as a numerical test that identifies phases<sup>11,14–18</sup>. A concrete demonstration that these quantities can in fact be measured to sufficient accuracy using current experimental techniques would turn these pure theoretical discussions into realistic physical observables, opening up entirely new possibilities in experimental studies of these phases.

We will thus focus on the  $Z_2$  topological order which can be realized as spin lattice models<sup>19,24</sup>. For the purpose of the current paper, we will in particular focus on the Kitaev realization<sup>19</sup>, whose lattice symmetry will be important in what follows. Generically, given a lattice model, it is a very difficult task to decipher the topological order it realizes, if at all. Ideally, one would hope to solve the lattice model exactly, and constructing anyonic excitation using string operators,

whose braiding properties can be computed. This is not always possible in more general models. The experimental goal we would like to achieve in this paper is the following: *assuming no further knowledge than the Hamiltonian itself, we will demonstrate how its modular matrices can be measured, thus uniquely identifying the topological order.*

We review the Kitaev  $Z_2$  toric code model briefly below, which is defined on an  $N \times N$  square lattice, as illustrated in Fig. 2, where each site resides a spin  $1/2$ <sup>24</sup>. In its simplest version, the Hamiltonian is written as

$$H_{Z_2} = - \sum_{\text{white plaquettes}} X_p - \sum_{\text{yellow plaquettes}} Z_p. \quad (1)$$

Here  $X_p = \prod_{j \in \partial p} \sigma_j^x$ ,  $Z_p = \prod_{j \in \partial p} \sigma_j^z$  are the plaquette operators that act on four spins surrounding a plaquette of  $p$ , and  $\sigma_j^{(x,z)}$  stand for Pauli operators. We note that the Kitaev toric code is related to the Wen-plaquette model by a basis change for lattices with an even number of sites along each row and column. In the Kitaev basis it preserves the full square lattice symmetries.

As mentioned above, this is an exactly solvable model because  $[X_p, Z_{p'}] = 0$  for all  $p$  and  $p'$ . The ground state subspace is given by

$$\mathcal{L} = \{|\psi_g\rangle \in \mathcal{H} : X_p|\psi_g\rangle = Z_p|\psi_g\rangle = |\psi_g\rangle \text{ for all } p\}. \quad (2)$$

The degeneracy of ground states depends on the genus  $g$  of Riemann surface, i.e.,  $D = 2^{2g}$ . If the Riemann surface has genus  $g$ , we can define  $2g$  noncontractible strings that connect to different topological sectors in  $\mathcal{L}$ . For example, on a torus it has four-fold degenerate ground states. And their ground states can be organized using two nontrivial closed string operators winding the two

independent cycles of the torus,  $\gamma_1$  and  $\gamma_2$  respectively,

$$|\psi_g^{(\nu_1, \nu_2)}\rangle = \mathcal{T}_x^{\nu_1}(\gamma_1) \mathcal{T}_x^{\nu_2}(\gamma_2) |\psi_g^{(0,0)}\rangle, \nu_1, \nu_2 = 0, 1. \quad (3)$$

Here the string operators are defined as  $\mathcal{T}_x(\gamma) = \prod_{j \in \gamma} \sigma_j^x$ . The initial topological sector  $|\psi_g^{(0,0)}\rangle$  of  $\mathcal{L}$  is given by the equal superposition of all contractible closed strings including no string (or say the string is a point).

In the experiment, we consider a unit cell (i.e., a  $2 \times 2$  square lattice) as our test system. The ground state of the Kitaev toric code model is a fixed point wave-function, whose topological properties are realized independently of lattice size<sup>24</sup>. Under the periodic boundary condition, the Hamiltonian can be written as

$$\hat{H}_{Z_2}^4 = -2(\sigma_1^x \sigma_2^x \sigma_3^x \sigma_4^x + \sigma_1^z \sigma_2^z \sigma_3^z \sigma_4^z). \quad (4)$$

The two nontrivial loop operators are  $\mathcal{T}_x(\gamma_1) = \sigma_1^x \sigma_4^x$  and  $\mathcal{T}_x(\gamma_2) = \sigma_1^x \sigma_2^x$ . Therefore, the four-fold degenerate ground states can be described as follows,

$$|\psi_g^{(0,0)}\rangle = (|0000\rangle + |1111\rangle)/\sqrt{2} \quad (5)$$

$$|\psi_g^{(0,1)}\rangle = (|0011\rangle + |1100\rangle)/\sqrt{2}$$

$$|\psi_g^{(1,0)}\rangle = (|0110\rangle + |1001\rangle)/\sqrt{2}$$

$$|\psi_g^{(1,1)}\rangle = (|0101\rangle + |1010\rangle)/\sqrt{2}.$$

The labels of these ground states refer to eigenvalues wrt string operators discussed in equation (3). Note that each state in Eq. (5) is a maximally entangled state. For our purpose however, *the*

*states could have been in any other basis without affecting our final results.* These are only chosen for convenience.

Figures 3a and 3b clearly illustrate that the  $\pi/2$  rotation and Dehn twist are equivalent to the experimental operations of  $\text{SWAP}_{13}$  and  $\text{SWAP}_{12}$ , respectively, which, auspiciously, keep the Hamiltonian (4) invariant. Working with the above basis of Eq. (5), the modular S and T matrices are obtained as follows,

$$S = \begin{pmatrix} 1 & 0 & 0 & 0 \\ 0 & 0 & 1 & 0 \\ 0 & 1 & 0 & 0 \\ 0 & 0 & 0 & 1 \end{pmatrix}, \quad T = \begin{pmatrix} 1 & 0 & 0 & 0 \\ 0 & 1 & 0 & 0 \\ 0 & 0 & 0 & 1 \\ 0 & 0 & 1 & 0 \end{pmatrix}. \quad (6)$$

The S,T matrices are not obtained in its standard form, in which the basis states should correspond to anyons that diagonalizes the T matrix. To recover the standard form, there is an algorithm that one could follow, as proposed in <sup>17</sup>, which begins with the diagonalization of the T matrix. Following the procedure, we can recover the modular matrices in their standard anyonic basis, which match exactly with the corresponding matrices of the "Toric Code modular tensor category" in Ref. <sup>26</sup>. We have thus demonstrated that the starting choice of basis states with which the experiments are performed is immaterial, since we can always recover the standard S,T matrices following <sup>17</sup>, as long as we have measured both S and T. Another important feature of topological orders in 2d are that, being described by unitary modular tensor categories, the S and T matrices, being fingerprints of these orders, take discrete set of values that are very different from each other for different orders. Therefore, if one were given the number of degenerate ground states on a

torus, it does not require exceeding accuracy in the measurement of S and T to identify uniquely the topological order involved.

Here it is also necessary to emphasize that although we only consider a unit cell as our testing system, the proposal for measuring S and T matrices is still feasible when extended to larger systems. The details on experimentally implementing S and T transformations and their complexity analysis are given in Supplementary Information. From the analysis, one can see that the measurement proposal acquires only polynomial complexity and is thus efficient.

Now we turn to the experimental realization to directly measure the modular matrices of the  $Z_2$  topological order. With the well-developed control technology<sup>28</sup>, nuclear magnetic resonance (NMR) has been widely utilized for many of the first demonstrations in quantum simulation<sup>29</sup>. In the experiment we employed three  $^{19}\text{F}$  spins and two  $^1\text{H}$  spins of 1-bromo-2,4,5-trifluorobenzene partially oriented in liquid crystal N-(4-methoxybenzaldehyde)-4-butylaniline (MBBA) as a 5-qubit NMR simulator. The molecular structure and the labeled qubits are shown in Fig. 4a. The first  $^{19}\text{F}$  spin (labeled by 0) is used as a probe qubit and the rest of the spins (labeled by  $1 \sim 4$ ) constitute the 4-qubit quantum register to simulate the system of a  $2 \times 2$  spin lattice. The experiment was carried out at 305 K on a Bruker AV-400 spectrometer. In this molecule, the effective couplings between nuclear spins originate from partially averaged dipolar interactions (DD-couplings) and scalar interactions (J-couplings). Since the chemical shift difference in each pair of spins is much higher than the effective coupling strength, the x and y components in DD-coupling interaction can be ignored by secular approximation<sup>30</sup>. Therefore, the effective Hamiltonian of this 5-qubit

system in doubly rotating frame is

$$H_{\text{NMR}} = \sum_{j=1}^5 \pi \nu_j \sigma_j^z + \sum_{1 \leq j < k \leq 5} \frac{\pi}{2} (J_{jk} + 2D_{jk}) \sigma_j^z \sigma_k^z, \quad (7)$$

with the related parameters shown in Fig. 4b.

The quantum circuit for measuring the modular matrices is shown in Fig. 4c. Using line-selective approach<sup>31</sup>, the quantum system was first prepared in the initial pseudo-pure state (PPS):  $\hat{\rho}_{00000} = \frac{1-\epsilon}{32} \mathbf{I} + \epsilon |00000\rangle\langle 00000|$ , with  $\mathbf{I}$  representing  $32 \times 32$  identity operator and  $\epsilon \approx 10^{-5}$  the polarization. Here we introduced a probe qubit for the interferometry, which is initialized in the superposition state (i.e.,  $\frac{1}{\sqrt{2}}(|0\rangle_0 + |1\rangle_0)$ ) by a Hadamard gate. It is easy to know that  $|0000\rangle$  happens to be the ground state of  $\hat{H}_0 = -\sum_{j=1}^4 \hat{\sigma}_z$ . We then adiabatically prepared the ground state (APGS)  $|\psi_g^{(0,0)}\rangle$  by varying the time-dependent Hamiltonian slowly enough,

$$\hat{H}(t) = [1 - s(t)] \hat{H}_0 + s(t) \hat{H}_{Z_2}, \quad (8)$$

where the parameter function  $s(t)$  increases monotonically from 0 at  $t = 0$  to 1 at  $t = T$ .  $s(t)$  was interpolated linearly with  $M$  discretized steps and the duration of each step is  $\tau = T/M$ . According to the adiabatic theorem<sup>32</sup>, the evolution time  $T$  obeys  $T = O(1/\Delta E_{\min})$ , where  $\Delta E_{\min}$  is the minimum energy gap encountered along the adiabatic evolution. The numerical simulated result shows that the theoretical fidelity of final state with respect to the true ground state  $|\psi_g^{(0,0)}\rangle$  reaches over 0.99 when  $M = 7$  and  $\tau = 0.43$ . In the equation (8), the Hamiltonian of the Kitaev toric code model can be efficiently simulated using the radio-frequency (RF) pulses and two-body interactions in the NMR system<sup>25</sup>. To reduce the accumulated pulse errors in the experiment, the shaped pulses calculated by the gradient ascent pulse engineering (GRAPE) method<sup>34</sup> are



applied to the adiabatic passage, with the length of each pulse being 22.5 ms. All the pulses have theoretical fidelities over 0.99, and are designed to be robust against the inhomogeneity of radio-frequency pulses. The details of adiabatic preparation of topological orders can be seen in Ref.

33.

The other topological sectors in  $\mathcal{L}$  can be realized by using two independent non-contractible string operators of  $\mathcal{T}_x^{\nu_1}(\gamma_1)\mathcal{T}_x^{\nu_2}(\gamma_2)$  acting on  $|\psi_g^{(0,0)}\rangle$  for  $\nu_{1/2} = 0, 1$ . After the experimental operation of  $\mathcal{O} = \text{S or T}$ , we measured the probe qubit and the final signal of NMR has the following form as

$$\text{Tr}(\hat{\rho}_f \hat{F}_0^+) = \frac{1}{2} \langle \psi_g^{(0,0)} | T_x^{\nu'_1}(\gamma_1) T_x^{\nu'_2}(\gamma_2) \mathcal{O} T_x^{\nu_1}(\gamma_1) T_x^{\nu_2}(\gamma_2) | \psi_g^{(0,0)} \rangle = \frac{1}{2} \langle \psi_g^{(\nu'_1, \nu'_2)} | \mathcal{O} | \psi_g^{(\nu_1, \nu_2)} \rangle, \quad (9)$$

where  $\hat{F}_0^+ = |0\rangle_0 \langle 1|$  is the observable operator of the probe qubit. The right side of equation (9) is the overlap of the degenerate ground states. Therefore, by taking different values of  $\nu_1, \nu_2, \nu'_1$  and  $\nu'_2$ , the representations of modular S and T matrices in  $\mathcal{L}$  were obtained. The main experimental results are shown in Fig. 5. From these results, we conclude that our experiments matches well with the theoretical predictions.

The  $^{19}\text{F}$  spectra for measuring all elements of modular S and T matrices are listed in Supplementary Information. The total experimental time is longer than  $T_2^*$  in spin-spin relaxation effect. Thus the final signal attenuated a lot, which is required to be normalized. The experimental errors mainly originated from the imperfection of GRAPE pulses (about 1%) and the statistical fluctuation of signal strength (around 2%). Through the diagonalization, the eigenvalues of  $T_{exp}$  are 0.95, 0.98, 0.98, -0.95, which correspond to the resulting statistics of topological spins for elementary

excitations of  $I$ ,  $e$ ,  $m$ ,  $f$ , respectively. The other topological properties, such as mutual statistics between anyons and fusion rules between anyons, can also be obtained from the resulting  $S$  and  $T$ . The experimental results show that the emergent state in such spin-lattice model is indeed the  $Z_2$  topological order.

To conclude, we presented the first experimental identification of topological order by measuring the modular  $S$  and  $T$  matrices. Some interesting properties such as quasiparticle statistics can be obtained from the resulting matrices. As a concrete example, this idea was demonstrated in a  $2 \times 2$  spin lattice of the Kitaev toric code model that realizes the  $Z_2$  topological order. Given the utility of the modular matrices in uniquely characterizing at least 2+1 dimensional topological orders, the success of our NMR systems open up future experimental avenues in identifying orders whose Hamiltonians may not be exactly solvable. It will be interesting to generalize our measurement method to characterize other topological phases in the future.

1. Landau, L. D. Theory of phase transformations. *Phys. Zs. Sowjet.* **11**, 26 (1937).
2. Ginzburg, V. L. & Landau, L. D. On the theory of superconductivity. *J. Exp. Eheur. Phys.* **20**, 1064 (1950).
3. Wen, X. G. Topological orders in rigid states. *Int. J. Mod. Phys. B.* **4**, 239 (1990).
4. Wen, X. G. *Quantum Field Theory of Many-Body Systems* (Oxford University Press, Oxford, 2004).

5. Wen, X. G. & Niu, Q. Ground-state degeneracy of the fractional quantum Hall states in the presence of a random potential and on high-genus Riemann surfaces. *Phys. Rev. B.* **41**, 9377 (1990).
6. Chen, X., Gu, Z. C. & Wen, X. G. Local unitary transformation, long-range quantum entanglement, wave function renormalization, and topological order. *Phys. Rev. B.* **82**, 155138 (2010).
7. Tsui, D. C., Stormer, H. L. & Gossard, A. C. Two-Dimensional magnetotransport in the extreme quantum limit. *Phys. Rev. Lett.* **48**, 1559 (1982).
8. Laughlin, R. B. Anomalous quantum Hall effect: an incompressible quantum fluid with fractionally charged excitations. *Phys. Rev. Lett.* **50**, 1395 (1983).
9. Keski-Vakkuri, E. & Wen, X. G. Ground state structure of hierarchical QH states on torus and modular transformation. *Int. J. Mod. Phys. B.* **07**, 4227 (1993).
10. Wen, X. G. Modular transformation and bosonic/fermionic topological orders in Abelian fractional quantum Hall states. Preprint at <http://arXiv.org/abs/1212.5121> (2012).
11. Zhang, Y., Grover, T., Turner, A., Oshikawa, M. & Vishwanath, A. Quasiparticle statistics and braiding from ground-state entanglement. *Phys. Rev. B.* **85**, 235151 (2012).
12. Zaletel, M. P., Mong, R. S. K. & Pollmann, F. Topological characterization of fractional quantum Hall ground states from microscopic hamiltonians. *Phys. Rev. Lett.* **110**, 236801 (2013).
13. Tu, H. H., Zhang, Y. & Qi, X. L. Momentum polarization: An entanglement measure of topological spin and chiral central charge. *Phys. Rev. B.* **88**, 195412 (2013).

14. Cincio, L. & Vidal, G. Characterizing topological order by studying the ground states on an infinite cylinder. *Phys. Rev. Lett.* **110**, 067208 (2013).
15. Mei, J. W. & Wen, X. G. Gutzwiller-projected parton wave functions. *Phys. Rev. B.* **91**, 125123 (2015).
16. Moridi, H. & Wen, X. G. Universal wave-function overlap and universal topological data from generic gapped ground states. *Phys. Rev. Lett.* **115**, 036802 (2015).
17. Liu, F. Z., Wang, Z. H., You, Y. Z. & Wen, X. G. Modular transformations and topological orders in two dimensions. Preprint at <http://arXiv.org/abs/1303.0829v2> (2014).
18. Jiang, S. H., Mesaros, A. & Ran, Y. Generalized modular transformations in (3+1)D topologically ordered phases and triple linking invariant of loop braiding. *Phys. Rev. X.* **4**, 031048 (2014).
19. Kitaev, A. Anyons in an exactly solved model and beyond. *Ann. Phys. (N.Y.)* **321**, 2 (2006).
20. Barkeshli, M., Bonderson, P., Cheng, M. & Wang, Z. H. Symmetry, Defects, and Gauging of Topological Phases. Preprint at <http://arXiv.org/abs/1410.4540v2> (2014).
21. Kitaev, A. & Preskill, J. Topological Entanglement Entropy. *Phys. Rev. Lett.* **96**, 110404 (2006).
22. Levin, M. & Wen, X. G. Detecting Topological Order in a Ground State Wave Function. *Phys. Rev. Lett.* **96**, 110405 (2006).

23. Jiang, H. C., Wang, Z. H. & Balents, L. Identifying topological order by entanglement entropy. *Nature Phys.* **8**, 902-905 (2012).
24. Wen, X. G. Quantum orders in an exact soluble model. *Phys. Rev. Lett.* **90**, 016803 (2003).
25. Peng, X. H., Luo, Z. H., Zheng, W. Q., Kou, S. P., Suter, D. & Du, J. F. Experimental implementation of adiabatic passage between different topological orders. *Phys. Rev. Lett.* **113**, 080404 (2014).
26. Rowell, E., Stong, R. & Wang, Z. H. *Comm. Math. Phys.* **292** no. 2, 343–389(2009).
27. Bonderson, P., Shtengel, K. & Slingerland, J. K. Probing non-abelian statistics with quasiparticle interferometry. *Phys. Rev. Lett.* **97**, 016401 (2006).
28. Ryan, C. A., Negrevergne, C., Laforest, M., Knill, E. & Laflamme, R. Liquid-state nuclear magnetic resonance as a testbed for developing quantum control methods. *Phys. Rev. A.* **78**, 012328 (2008).
29. Feynman, R. P. Simulating physics with computers. *Int. J. Theor. Phys.* **21**, 467 (1982).
30. Dong, R. Y. *Nuclear Magnetic Resonance of Liquid Crystals* (Springer, New York, 1997).
31. Peng, X. H., Zhu, X., Fang, X., Feng, M., Gao, K., Yang, X. & Liu, M. Preparation of pseudo-pure states by line-selective pulses in nuclear magnetic resonance. *Chem. Phys. Lett.* **340**, 509 (2001).
32. Messiah, A. *Quantum Mechanics* (Wiley, New York, 1976).

33. Luo, Z. H., Li, Jun., Li, Z. K. Hung, L. X., Wan, Y. D., Peng, X. H., & Du, J. F., Experimental preparation of topologically ordered states via adiabatic evolution. In preparation (2016).
34. Khaneja, N., Reiss, T., Kehlet, C., Schulte Herbrüggen, T. & Glaser, S. J., Optimal Control of Coupled Spin Dynamics: Design of NMR Pulse Sequences by Gradient Ascent Algorithms. *J. Magn. Reson.* **172**, 296 (2005).

**Acknowledgements** We thank Xiaogang Wen and Bei Zeng for helpful discussions. This work is supported by NKBRP (2013CB921800 and 2014CB848700), the National Science Fund for Distinguished Young Scholars (11425523), the National Natural Science Foundation of China (Grants No. 11375167, No. 11227901, No. 11575173, and No. 91021005), the Strategic Priority Research Program (B) of the CAS (Grant No. XDB01030400), and RFDP (20113402110044). YW acknowledges the support from the John Templeton foundation No. 39901. This research was supported in part by Perimeter Institute for Theoretical Physics. Research at Perimeter Institute is supported by the Government of Canada through the Department of Innovation, Science and Economic Development Canada and by the Province of Ontario through the Ministry of Research, Innovation and Science. LYH would like to acknowledge support by the Thousand Young Talents Program, and Fudan University.

**Competing Interests** The authors declare that they have no competing financial interests.

**Correspondence** Correspondence and requests for materials should be addressed to X. H. P.(xhpeng@ustc.edu.cn) or L. Y. H. (Lyhung@fudan.edu.cn) or Y. D. W. (ydw@fudan.edu.cn).

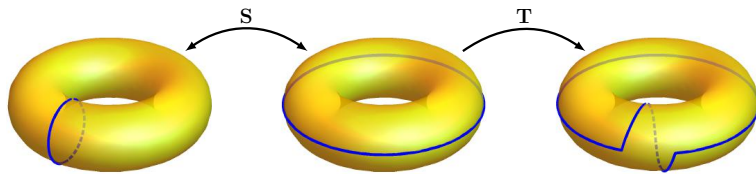


**Figure 1:** The physical diagrams of the modular S and T transformations corresponding to  $\pi/2$  rotation and Dehn twist on a torus, respectively.

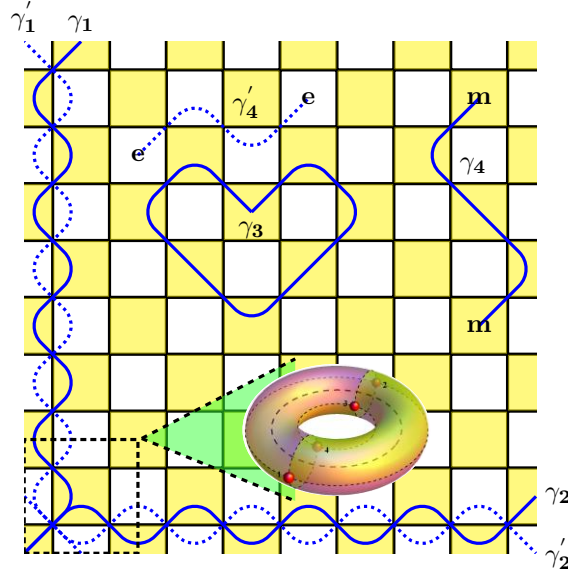


**Figure 2:** The Wen-plaquette spin-lattice model on a torus. When  $N$  is even, there exist two sublattice denoted by white and yellow. The blue solid strings ( $\gamma_1 \sim \gamma_4$ ) and their dual dashed strings ( $\gamma'_1 \sim \gamma'_4$ ) are defined in the yellow sublattice and in the white sublattice, respectively.  $e$  and  $m$  represent the elementary excitations (anyons): electric charge and magnetic vortex, which in pairs generated by open string operators. The black dashed box is an unit cell of square lattice and form a torus under the periodic boundary condition. The red spheres represent spins.



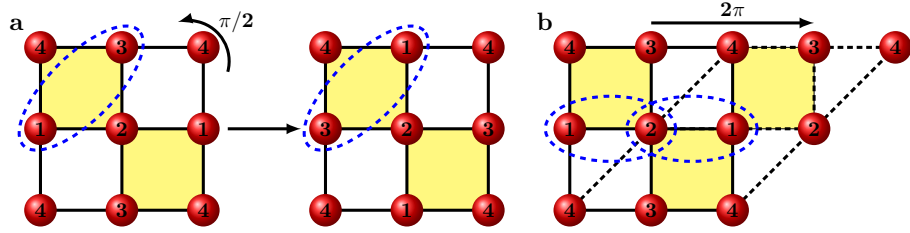


**Figure 3:** Physically, **a**,  $\pi/2$  rotation and **b**, Dehn twist or a shear deformation on a torus in a  $2 \times 2$  square lattice are equivalent to  $\text{SWAP}_{13}$  and  $\text{SWAP}_{12}$  operations, respectively.

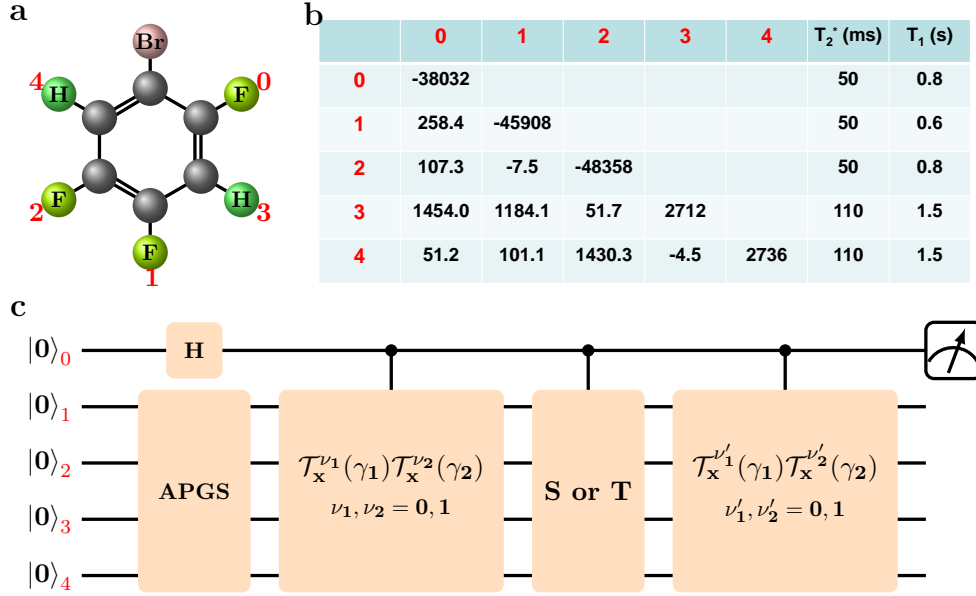


**Figure 4:** **a**, Molecular structure of the 1-bromo-2,4,5-trifluorobenzene. **b**, Relevant parameters measured at  $T=305$  K. The diagonal and off-diagonal elements represent the chemical shifts  $\nu_i$  and effective coupling constants  $(J_{jk} + 2D_{jk})$  in units of Hz, respectively. **c**, Quantum circuit for measuring the modular S and T matrices. H stands for the Hadamard gate acting on the auxiliary qubit. The system (spins 1 ~ 4) is adiabatically prepared into the ground state  $|\psi_g^{(0,0)}\rangle$ , labeled by APGS, and then performed three controlled operations in turn. Finally the information of S and T can be extracted via measuring the auxiliary qubit.

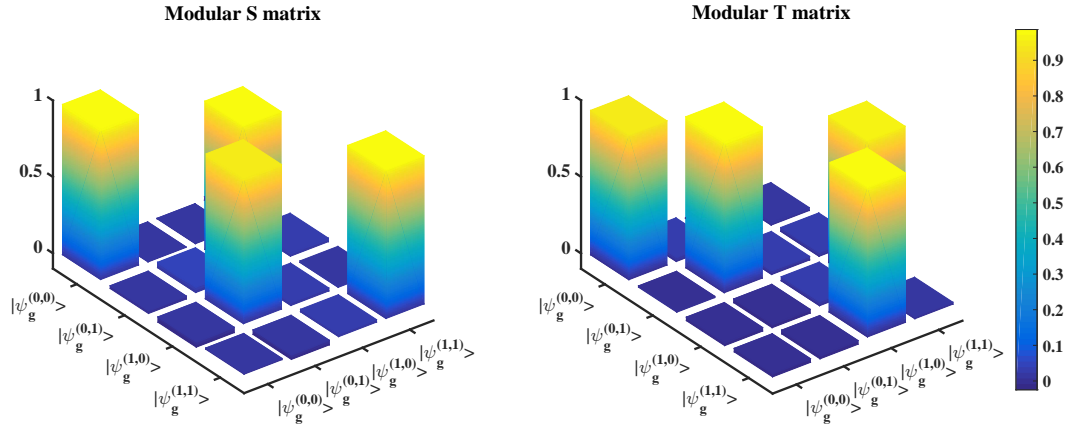


**Figure 5:** The experimental results of measuring modular S and T matrices in a given Wen-plaquette model.

## SUPPLEMENTARY INFORMATION

for

### Identifying topological order by measuring modular matrices

Zhihuang Luo<sup>1,2</sup>, Jun Li<sup>2</sup>, Zhaokai Li<sup>1</sup>, Ling-Yan Hung<sup>3,4,5\*</sup>, Yidun Wan<sup>3,4,5,6\*</sup>, Xinhua Peng<sup>1,7\*</sup>,  
& Jiangfeng Du<sup>1,7</sup>

#### 1 The modular S and T matrices

The topological properties of 2+1 dimension quantum systems with an energy gap can be described by topological quantum field theory (TQFT) or unitary modular tensor category<sup>19,20</sup>. We begin with a finite set  $\mathcal{C}$  of quasiparticle types or anyons labeled by  $a, b, c, \dots \in \mathcal{C}$ . The two major concepts in anyon models are fusion and braiding, which can be represented diagrammatically by oriented, labeled particle worldlines, and are unaffected by smooth deformations in which the lines do not intersect. The fusion rules are specified as  $a \times b = \sum_{c \in \mathcal{C}} N_{ab}^c c$ , where the integer  $N_{ab}^c$  is the dimension of the Hilbert space of particles of type  $a$  and  $b$  restricted to have total anyonic charge  $c$ . The braiding operator of  $a$  and  $b$  is represented diagrammatically by

$$\begin{array}{c} a \quad b \\ \diagdown \quad \diagup \\ \bigcirc \quad \mu \\ \diagup \quad \diagdown \\ c \end{array} = \sum_{\nu} [R_c^{ab}]_{\mu\nu} \begin{array}{c} a \quad b \\ \diagdown \quad \diagup \\ \bigcirc \quad \nu \\ \diagup \quad \diagdown \\ c \end{array}. \quad (S1)$$

The above finite set  $\mathcal{C}$ , fusion rules  $N_{ab}^c$  and braiding rules  $R_c^{ab}$  uniquely determine the anyon models. The other physical quantities or properties can be derived from these three definitions. For example, according to braiding, we can define an important quantity, i.e., topological spin as,

$$\theta_a = \theta_{\bar{a}} = \sum_{c, \mu} \frac{d_c}{d_a} [R_c^{aa}]_{\mu\mu} = \frac{1}{d_a} \bigcirc_a. \quad (S2)$$

We now give the algebraic definitions of the modular S and T matrices:

$$S_{ab} = \mathcal{D}^{-1} \sum_c N_{\bar{a}b}^c \frac{\theta_c}{\theta_a \theta_b} d_c = \frac{1}{\mathcal{D}} \text{a} \begin{array}{c} \circlearrowleft \\ \circlearrowright \end{array} \text{b}, \quad (\text{S3})$$

and  $T_{ab} = \theta_a \delta_{ab}$ , where  $\mathcal{D} = \sqrt{\sum_a d_a^2}$  is total quantum dimension and  $d_a$  the quantum dimension of quasiparticle type  $a$  is the value of a single loop of that type, that is,

$$d_a = d_{\bar{a}} = \text{a} \begin{array}{c} \circlearrowleft \\ \circlearrowright \end{array}. \quad (\text{S4})$$

From the above algebraic theory of anyons or unitary modular tensor category, it is not difficult to find that the element of modular S matrix determines the mutual statistics of quasiparticles, while the element of T matrix determines the topological spin. We can further reconstruct the fusion coefficients from the S matrix according to the Verlinde formula, i.e.,

$$N_{ab}^c = \sum_{x \in \mathcal{C}} \frac{S_{ax} S_{bx} S_{cx}^*}{S_{0x}}. \quad (\text{S5})$$

The fusion rules and braiding rules reflect two major algebraic structures of anyons. The topological properties of topologically ordered states are associated to elementary excitations, i.e., anyons. Therefore, S and T matrices provide a complete description and can be taken as the nonlocal order parameters of topological phases.

To better understand this point, we list several examples for identifying different topological

orders using the modular matrices<sup>17</sup>. For  $Z_2$  states ( $\eta = 1$ ), the numerical results give

$$S = \begin{pmatrix} 1 & 0 & 0 & 0 \\ 0 & 0 & 1 & 0 \\ 0 & 1 & 0 & 0 \\ 0 & 0 & 0 & 1 \end{pmatrix}, \quad T = \begin{pmatrix} 1 & 0 & 0 & 0 \\ 0 & 1 & 0 & 0 \\ 0 & 0 & 0 & 1 \\ 0 & 0 & 1 & 0 \end{pmatrix}. \quad (\text{S6})$$

Choosing the eigenstates of T matrix as the basis, we get the standard S and T matrices as follows,

$$S_{\text{standard}} = \begin{pmatrix} 1 & 1 & 1 & 1 \\ 1 & 1 & -1 & -1 \\ 1 & -1 & 1 & -1 \\ 1 & -1 & -1 & 1 \end{pmatrix}, \quad T_{\text{standard}} = \begin{pmatrix} 1 & 0 & 0 & 0 \\ 0 & 1 & 0 & 0 \\ 0 & 0 & 1 & 0 \\ 0 & 0 & 0 & -1 \end{pmatrix}. \quad (\text{S7})$$

The results show that there are four different types of quasiparticles with statistical angles,

$$(e^{i\theta_i}) = (1, 1, 1, -1). \quad (\text{S8})$$

These agree with the toric code model and wen-plaquette model.

For  $Z_2$  states ( $\eta = -1$ ), we have in standard forms,

$$S_{\text{standard}} = \frac{1}{\sqrt{2}} \begin{pmatrix} 1 & 1 \\ 1 & -1 \end{pmatrix} \otimes \frac{1}{\sqrt{2}} \begin{pmatrix} 1 & 1 \\ 1 & -1 \end{pmatrix}, \quad (\text{S9})$$

$$T_{\text{standard}} = \begin{pmatrix} 1 & 0 \\ 0 & i \end{pmatrix} \otimes \begin{pmatrix} 1 & 0 \\ 0 & -i \end{pmatrix},$$

there are also four different types of quasiparticles with different statistical angles,

$$(e^{i\theta_i}) = (1, 1, i, -i). \quad (\text{S10})$$

The doubled structures match exactly with the "double semion" model.

For the fibonacci states,

$$S_{\text{standard}} = \frac{5 - \sqrt{5}}{\sqrt{10}} \begin{pmatrix} 1 & \frac{1+\sqrt{5}}{2} \\ \frac{1+\sqrt{5}}{2} & -1 \end{pmatrix} \otimes \begin{pmatrix} 1 & \frac{1+\sqrt{5}}{2} \\ \frac{1+\sqrt{5}}{2} & -1 \end{pmatrix}, \quad (\text{S11})$$

$$T_{\text{standard}} = \begin{pmatrix} 1 & 0 \\ 0 & e^{-i\frac{4\pi}{5}} \end{pmatrix} \otimes \begin{pmatrix} 1 & 0 \\ 0 & e^{i\frac{4\pi}{5}} \end{pmatrix},$$

which has four types of quasiparticles with statistical angles,

$$(e^{i\theta_i}) = (1, 1, e^{i\frac{4\pi}{5}}, e^{-i\frac{4\pi}{5}}). \quad (\text{S12})$$

The above examples show that the modular matrices (up to an unitary transformation) form a complete and one-to-one characterization of exact topological orders.

## 2 Experimental operations for implementing modular S and T transformations

For a  $N \times N$  square lattice of Wen-plaquette model, the implementation of modular S and T transformations can be used a sequence of SWAP operations in experiments. Here we give a general procedure for their experimental operations and further analyze their complexities. Because the modular S and T transformations correspond to  $\pi/2$  rotation and a shear, they are equivalent to a series of permutations with length 4 and  $N$ , respectively, as illustrated in Figs. S2a and

S2b. For example, four associated points in Fig. S2a form a cycle under a  $\pi/2$  rotation, i.e.,  $(a_{i,j}, a_{j,-i}, a_{-i,-j}, a_{-j,i})$ , and  $N$  associated points  $(a_{-n,j} = a_{n,j}, n = [(N+1)/2])$  in Fig. S2b form a permutation under a shear, i.e.,  $\begin{pmatrix} a_{-n,j} & a_{-n+1,j} & \cdots & a_{n-2,j} & a_{n-1,j} \\ a_{j,j} & a_{j+1,j} & \cdots & a_{j-2,j} & a_{j-1,j} \end{pmatrix}$ , which can be decomposed as the product of  $n_m (= \gcd(n+j, N))$ ,  $\gcd$  means the greatest common divisor) cycles of length  $m = N/n_m$ . According to group theory, any cycle can be written as the product of transpositions or SWAP operations between two elements. We thus have

$$(a_{i,j}, a_{j,-i}, a_{-i,-j}, a_{-j,i}) = (a_{i,j}, a_{-j,i})(a_{i,j}, a_{-i,-j})(a_{i,j}, a_{j,-i}), \quad (\text{S13})$$

and

$$\begin{aligned} & \begin{pmatrix} a_{-n,j} & a_{-n+1,j} & \cdots & a_{n-2,j} & a_{n-1,j} \\ a_{j,j} & a_{j+1,j} & \cdots & a_{j-2,j} & a_{j-1,j} \end{pmatrix} \\ &= \prod_{k=0}^{n_m-1} (a_{-n+k,j}, a_{j+k,j}, \cdots, a_{(m-2)(n+j)-n+k \bmod N,j}, a_{(m-1)(n+j)-n+k \bmod N,j}) \\ &= \prod_{k=0}^{n_m-1} (a_{-n+k,j}, a_{(m-1)(n+j)-n+k \bmod N,j})(a_{-n+k,j}, a_{(m-2)(n+j)-n+k \bmod N,j}) \cdots (a_{-n+k,j}, a_{j+k,j}). \end{aligned} \quad (\text{S14})$$

We now can calculate the number of experimental operations. For implementing a S transformation, it needs  $\#(\text{SWAP}) = 3(n^2 - 1) + 3(n - 1) + 1 = 3n^2 + 3n + 5$ . Here we consider the situation on the border separately, because it is different a little from that in the body of lattice. For implementing a T transformation, it needs  $\#(\text{SWAP}) = \sum_{j=-n+1}^{n-1} (m - 1)n_m = N^2 - N - \sum_{j=-n+1}^{n-1} \gcd(n+j, N)$ . So the implementation of modular S and T transformations only requires polynomial SWAP gates.



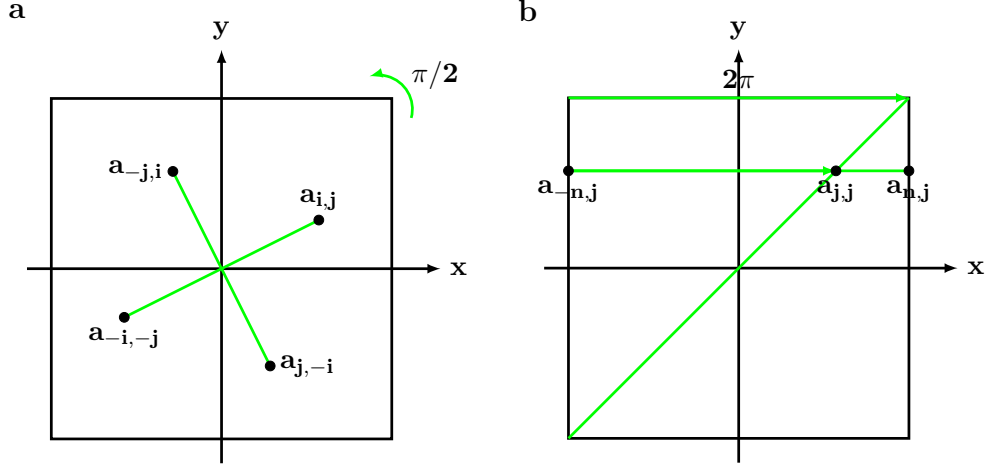


**Figure S1:** The diagrams for implementing a  $\pi/2$  rotation and a shear, respectively.

### 3 Decomposition of controlled string operation and controlled modular matrix

It can be found that the string operations and modular matrices are the product of  $\sigma_x$  and SWAP operations, respectively. On the other hand, we know that a controlled-U gate is equivalent to the product of a controlled-B gate and a controlled-A gate, if U satisfy that  $U=AB$ . Therefore, the controlled string operations and the controlled modular matrices can be decomposed into a series of CNOT gates and Toffoli gates, respectively. For instance, in our experimental proposal (i.e., only considering a  $2 \times 2$  lattice), the decomposition of controlled string operation and controlled modular S or T matrix are shown in Figs. S2a and S2b. It is not difficult to get the result that it requires  $\mathcal{O}(N)$  CNOT gates to implement a controlled string operation and  $3\#(\text{SWAP})$  Toffoli gates to implement a controlled modular matrix for a  $N \times N$  lattice. The decomposition complexity is polynomial, which means that the measurement of modular S and T matrices is an efficient approach when extended to larger systems..

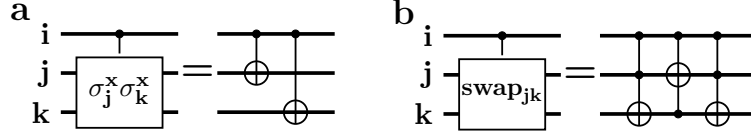


**Figure S2: The decomposition of a, controlled string operation and b, controlled S or T matrix** for our experimental proposal.

#### 4 Experimental spectra and results

The equilibrium  $^{19}\text{F}$  spectrum of 1-bromo-2,4,5-trifluorobenzene is illustrated at the top of Fig. S3. The first  $^{19}\text{F}$  nuclear spin (labeled by 0) is used for interference measurement of modular matrices. The beautiful spectrum of PPS  $\rho_{00000}$  at the bottom of Fig. S3 shows that we can achieve a high accuracy in experiments. Its signal attenuation a lot is due to decoherence. The length of shape pulse used for preparing PPS  $\rho_{00000}$  was 37.5 ms, which is considerable with  $T_2^*$ .

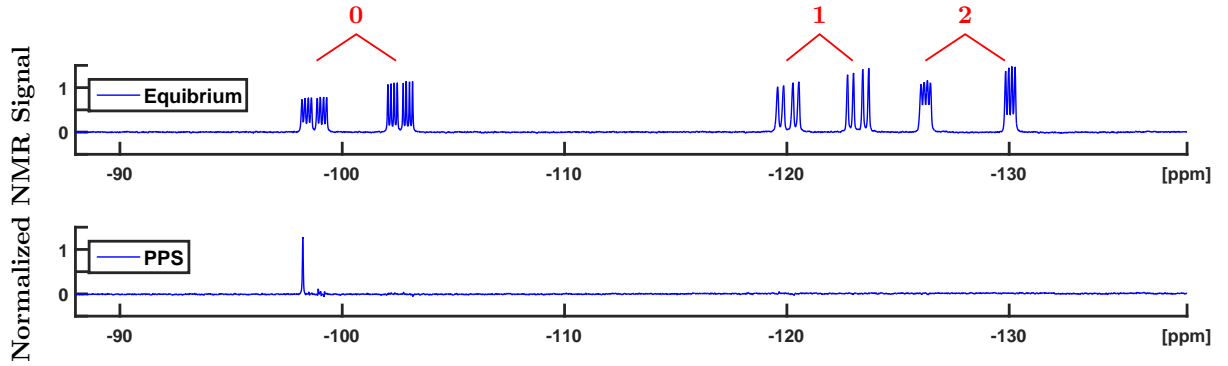


**Figure S3: The experimental  $^{19}\text{F}$  spectra of thermal equilibrium state (at the top) and PPS  $\rho_{00000}$  (at the bottom).** In the experiment, we only measure the signal on first  $^{19}\text{F}$  nuclear spin (i.e., 0-qubit).

Figure S4 shows the  $^{19}\text{F}$  spectra for measuring all elements of modular S and T matrices.

The experimental results are listed in the following,

$$S_{\text{exp}} = \begin{pmatrix} 0.98 & 0.00 & 0.00 & 0.02 \\ -0.02 & 0.03 & 0.97 & 0.02 \\ -0.03 & 0.95 & 0.02 & 0.01 \\ -0.01 & -0.03 & 0.02 & 0.97 \end{pmatrix}, \quad (\text{S15})$$

and,

$$T_{\text{exp}} = \begin{pmatrix} 0.94 & 0.03 & 0.00 & 0.02 \\ -0.01 & 0.99 & 0.02 & 0.02 \\ -0.02 & -0.02 & 0.03 & 0.96 \\ -0.02 & -0.02 & 0.98 & 0.01 \end{pmatrix}. \quad (\text{S16})$$

They are not unitary due to the inevitable errors of measurement. These results can be further processed using optimal searching algorithm, i.e., to find a unitary matrix that is the most close to the experimental matrix. The experimental unitary S and T matrices by processing are

$$S_{\text{exp}}^p = \begin{pmatrix} 0.9997 & 0.0162 & 0.0072 & 0.0166 \\ -0.0074 & 0.0083 & 0.9999 & 0.0035 \\ -0.0164 & 0.9996 & -0.0085 & 0.0212 \\ -0.0162 & -0.0215 & -0.0035 & 0.9997 \end{pmatrix}, \quad (\text{S17})$$

and,

$$T_{\text{exp}}^p = \begin{pmatrix} 0.9995 & 0.0176 & 0.0141 & 0.0223 \\ -0.0185 & 0.9992 & 0.0237 & 0.0250 \\ -0.0219 & -0.0255 & 0.0066 & 0.9994 \\ -0.0135 & -0.0238 & 0.9996 & 0.0075 \end{pmatrix}. \quad (\text{S18})$$

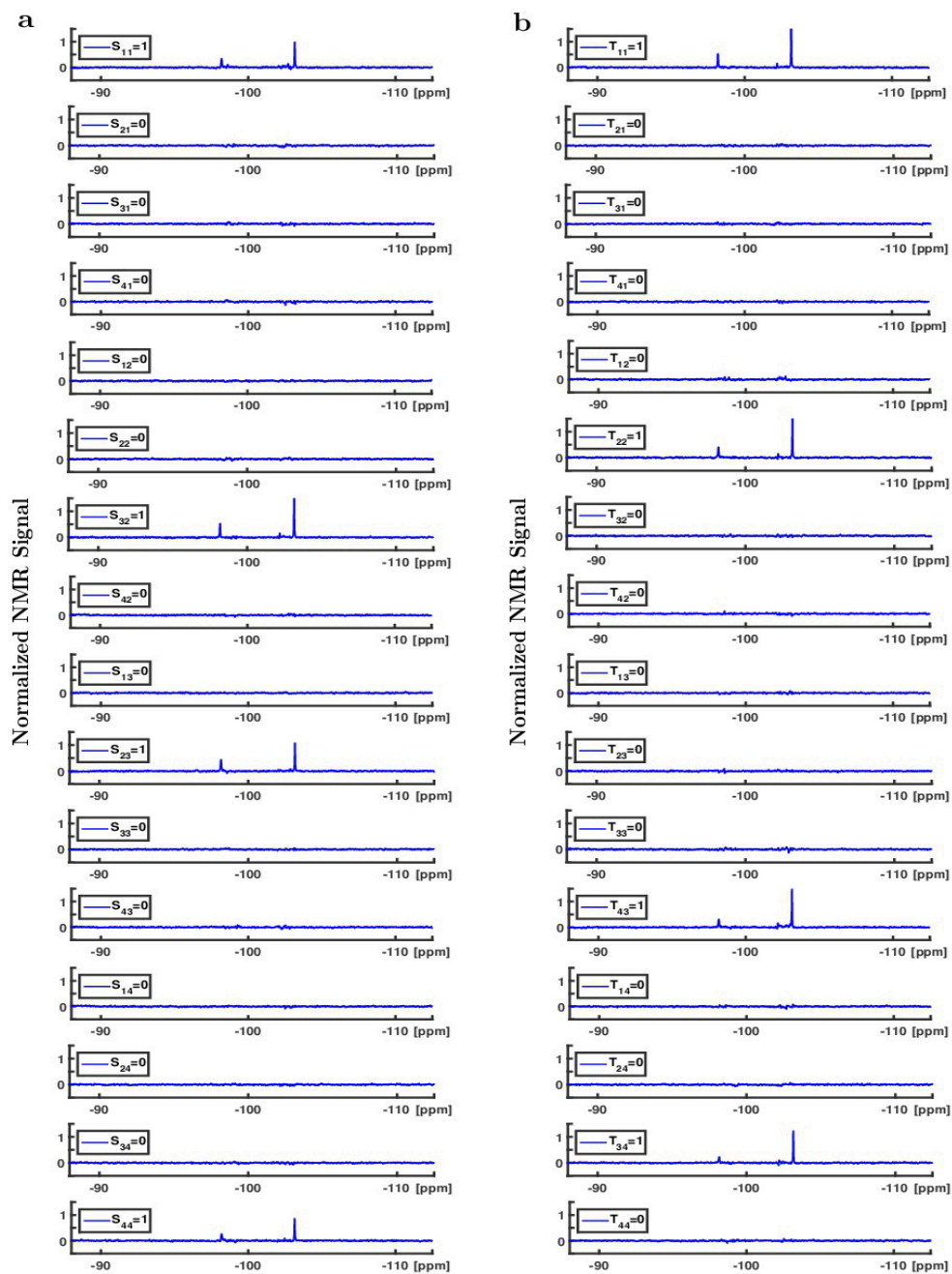


**Figure S4:** The  $^{19}\text{F}$  spectra for measuring all elements of modular S and T matrices.